Volume 17
Number 2
14 January 2026
Pages 675–1382

Chemical Science

rsc.li/chemical-science

ISSN 2041-6539

ROYAL SOCIETY OF CHEMISTRY

EDGE ARTICLE

Ziyang Song, Lihua Gan, Mingxian Liu *et al.*
Highly zincophilic-hydrophobic polyzwitterionic hydrogel electrolyte with strong electronegative sulfobetaine-carboxyl motifs for ultrastable zinc-ion batteries

Chemical Science

ROYAL SOCIETY OF CHEMISTRY

EDGE ARTICLE

View Article Online
View Journal | View Issue

Cite this: *Chem. Sci.*, 2026, **17**, 906

All publication charges for this article have been paid for by the Royal Society of Chemistry

Highly zincophilic-hydrophobic polyzwitterionic hydrogel electrolyte with strong electronegative sulfobetaine-carboxyl motifs for ultrastable zinc-ion batteries

Jia Zhou,[a] Qi Huang,[d] Yaokang Lv,[e] Ziyang Song,*[b] Lihua Gan*[ac] and Mingxian Liu*[ac]

Polyzwitterionic hydrogel electrolytes with good anionic affinity and a well-aligned Zn^{2+} deposition effect are regarded as potential alternatives for propelling zinc-ion batteries (ZIBs). However, their hydrophilic molecular chains show relatively low zincophility and easily transfer H_2O molecules to the Zn surface, resulting in interfacial Zn corrosion and dendrites. Here we design highly zincophilic-hydrophobic polyzwitterionic hydrogel electrolyte (SC-PAM) *via* the crosslinking of zwitterionic sulfobetaine and carboxyl-rich carboxylated chitosan for ultrastable ZIBs. The zincophilic $-SO_3^-$ motifs of zwitterionic sulfobetaine in SC-PAM afford highly Zn^{2+}-selective migration channels and homogenize Zn^{2+} flux with a high transference number of 0.90. Meanwhile, strong electronegative carboxyl groups (C=O) in carboxylated chitosan strongly anchor H_2O molecules *via* rich H-bonding interactions to establish a hydrophobic interfacial layer, which shields direct contact between H_2O solvent and the Zn anode to avoid Zn corrosion. As a consequence, the Zn||SC-PAM||Cu cell exhibits a high average coulombic efficiency of 99.7% during 7600 cycles, while the Zn||SC-PAM||Zn cell shows ultrastable cycling exceeding 7500 hours. Significantly, SC-PAM can be further leveraged to design a state-of-the-art Zn||SC-PAM||V_2O_5 full battery with high capacity (372 mAh g^{-1}), large-current tolerance (15 A g^{-1}), and ultralong cycle life (5000 cycles). This work extends the structural engineering landscape of zincophilic-hydrophobic polyzwitterionic hydrogel electrolytes for advanced ZIBs.

Received 13th November 2025
Accepted 16th December 2025

DOI: 10.1039/d5sc08853d

rsc.li/chemical-science

Introduction

Aqueous zinc-ion batteries (ZIBs) have been proven to be attractive solutions for large-scale energy storage applications because of their intrinsic advantages including high safety, low cost, and environmental compatibility.[1–3] A key advantage of ZIBs arises from the Zn metal anode, which exhibits a low redox potential (−0.76 V *vs.* SHE), a high theoretical capacity (820 mAh g^{-1}), and excellent aqueous compatibility.[4,5] Despite the above merits, ZIBs still face fundamental challenges with several critical technical issues, which include dendrite growth, the Zn corrosion reaction and the hydrogen evolution reaction (HER).[6–8] These issues originate from the undesirable interfacial reactions between Zn anodes and aqueous electrolytes.[9–11] Although aqueous electrolytes offer high ionic conductivity suitable for high-power output, a large amount of free water molecules would accelerate the HER, leading to poor interfacial stability. In contrast, non-aqueous electrolytes can effectively suppress the HER and enhance low-temperature performance, but their practicality is limited by significantly reduced ionic conductivity and high interfacial impedance.[12–14] Thus, there is an urgent need to design new-type electrolytes that can protect the Zn anode from water-induced corrosion while simultaneously delivering enhanced Zn^{2+} ion transport kinetics.

Hydrogel electrolytes have garnered considerable attention because they integrate the high ionic conductivity of aqueous electrolytes and the low volatility of organic systems, along with the ability to form conformal interfacial contact through flexible polymer networks.[15–17] Compared to conventional aqueous electrolytes, the restricted water environment within hydrogel electrolytes could confer better Zn anode cyclability.[18,19]

[a]*Shanghai Key Lab of Chemical Assessment and Sustainability, School of Chemical Science and Engineering, Tongji University, 1239 Siping Rd., Shanghai, 200092, P. R. China. E-mail: ganlh@tongji.edu.cn; liumx@tongji.edu.cn*

[b]*State Key Laboratory of Pollution Control and Resource Reuse, College of Environmental Science and Engineering, Advanced Research Institute, Tongji University, 1239 Siping Rd., Shanghai, 200092, P. R. China. E-mail: songziyang@tongji.edu.cn*

[c]*State Key Laboratory of Cardiovascular Diseases and Medical Innovation Center, Shanghai East Hospital, School of Medicine, Tongji University, 150 Jimo Rd., Shanghai 200120, P. R. China*

[d]*Institute for Electric Light Sources, School of Information Science and Technology, Fudan University, 220 Songhu Rd., Shanghai 200438, P. R. China*

[e]*College of Chemical Engineering, Zhejiang University of Technology, 18 Chaowang Rd., Hangzhou 310014, P. R. China*

Nevertheless, their practical application still faces challenges, such as sluggish Zn^{2+} ion migration kinetics and inefficient desolvation of hydrated Zn^{2+} ions, which limit the effectiveness of the inhibitory effect.[20,21] Recently, researchers have developed polycation- or polyanion-functionalized hydrogel electrolytes to overcome these limitations. Specifically, the positive electric field present in polycationic hydrogel electrolytes effectively immobilizes anions to enhance Zn^{2+} ion mobility and promote oriented Zn deposition, thereby inhibiting dendrite growth and mitigating tip effects.[22,23] Nevertheless, the hydrophilic segments of polycationic hydrogel electrolytes still struggle to effectively suppress water-induced side reactions. In contrast, polyanionic hydrogel electrolytes with zincophilic groups facilitate homogeneous Zn^{2+} ion transport and exhibit improved structural robustness.[24,25] However, excessively strong anionic interactions restrict the migration kinetics of Zn^{2+} ions.

To conquer the shortcomings of polycationic and polyanionic hydrogel electrolytes and leverage their relative functional advantages, polyzwitterionic hydrogel electrolytes have been developed, which form well-defined anion/cation migration channels *via* electrostatic interactions between electropositive and electronegative groups.[26–28] Polyzwitterionic hydrogel electrolytes thus promote rapid Zn^{2+} migration and homogenize Zn^{2+} flux to achieve well-aligned Zn deposition, leading to stable electrochemical processes during the operation of ZIBs.[29–31] As an example, the Qiu group prepared sulfobetaine-functionalized polyzwitterionic hydrogel electrolytes to facilitate rapid ion migration with a high Zn^{2+} transference number of 0.84.[32] The Zn‖Zn battery thus exhibited stable cycling for 400 h at 2 mA cm^{-2} and the Zn‖Cu battery maintained an average coulombic efficiency of 99.4% over 700 cycles. These results broaden the design horizons of polyzwitterionic hydrogel electrolytes for efficient ZIBs. Despite significant progress, polyzwitterionic chains with weak-electronegative sulfonate components are generally hydrophilic and can transport water molecules to directly come into contact with the Zn surface, which triggers the growth of Zn dendrites and parasitic side reactions over extended cycling. Thus, attempts are still required for further success in unlocking the intrinsic functional limitations of polyzwitterionic hydrogel electrolytes, thereby achieving better zincophility and hydrophobicity towards interfacial corrosion-resistant and dendrite-free Zn anodes for superior ZIBs.

In this work, we design a highly zincophilic-hydrophobic polyzwitterionic hydrogel electrolyte (SC-PAM) to guide uniform Zn^{2+} flux and effectively suppress Zn corrosion, thereby significantly enhancing the stability of Zn anodes. SC-PAM was fabricated through the crosslinking of zwitterionic sulfobetaine and carboxyl-rich carboxylated chitosan. The zincophilic $-SO_3^-$ functional groups of zwitterionic sulfobetaine in SC-PAM provide selective Zn^{2+} transport channels and promote uniform Zn^{2+} deposition with a high transference number of 0.90. In addition, the strongly electronegative carboxylated chitosan in SC-PAM forms a hydrophobic layer on the Zn anode surface through H-bonding interactions, which protects the Zn anode from direct water contact and efficiently restricts water molecule activity, thereby inhibiting water-induced corrosion. Consequently, the Zn‖SC-PAM‖Cu cell demonstrates an average coulombic efficiency as high as 99.7% over 7600 cycles, while the Zn‖SC-PAM‖Zn cell achieves excellent cyclability exceeding 7500 hours. Besides, SC-PAM can be further leveraged to design an advanced Zn‖SC-PAM‖V_2O_5 full battery with high capacity and cycling stability among previously reported batteries of the same type. These findings give new insights into the design of zincophilic-hydrophobic polyzwitterionic hydrogel electrolytes and provide a good starting point for advanced ZIBs.

Results and discussion

The electrochemical mechanism of zincophilic-hydrophobic SC-PAM is shown in Fig. 1. Specifically, the conventional polyacrylamide (PAM) hydrogel electrolyte exhibits inhomogeneous charge distribution on the Zn anode surface and faces the high desolvation energy of hydrated Zn^{2+} ions during repeated plating/stripping processes (Fig. 1a), leading to Zn corrosion and uncontrolled dendritic growth. In contrast, the incorporation of [2-(methacryloyloxy)ethyl]dimethyl-(3-sulfopropyl) (MDS, zwitterionic sulfobetaine) into the PAM skeleton (denoted as S-PAM) immobilizes anionic carriers, effectively facilitating rapid Zn^{2+} migration and homogenizing the interfacial electric field, which ultimately suppresses Zn dendrite growth (Fig. 1b). However, the inherent hydrophilicity of polymeric chains of S-PAM permits water molecules to direct exposure to the Zn anode, leading to Zn corrosion and gradually accelerating the formation of dendrites during long-term cycling. Significantly, SC-PAM is designed by the crosslinking of zwitterionic MDS and carboxyl-rich carboxylated chitosan (CC) as the polyzwitterionic hydrogel electrolyte for ZIBs. The zincophilic $-SO_3^-$ groups of zwitterionic sulfobetaine in SC-PAM are expected to provide selective Zn^{2+} transport pathways and boost uniform Zn^{2+} deposition (Fig. 1c). Meanwhile, the strongly electronegative carboxylated chitosan in SC-PAM can form a hydrophobic layer on the Zn anode surface through H-bonding interactions, which is beneficial for preventing the Zn anode from direct water contact and efficiently restricting water molecule activity, thereby inhibiting water-induced corrosion to greatly improve the Zn anode cyclability.

The structure and composition of SC-PAM polyzwitterionic hydrogel electrolyte were probed by Fourier-transform infrared (FT-IR) spectroscopy and X-ray photoelectron spectroscopy (XPS). Characteristic peaks at 1025 and 1400 cm^{-1} could be observed, corresponding to C–OH and O–C=O groups for CC, respectively. The characteristic peaks at 1039 and 1190 cm^{-1} were assigned to S=O and $-SO_3^-$ groups for MDS (Fig. 2a and S1).[33,34] In addition, XPS spectra show C 1s characteristic peaks of C–C, C–O/C–N and C=O (Fig. 2b and S2a) and O 1s peaks of C–O and C=O (Fig. 2c and S2b).[35] In addition, X-ray diffraction patterns of the four hydrogel electrolytes show broad diffraction peaks centered at 27°, indicating typical amorphous and non-crystalline polymer structures (Fig. 2d). This disordered feature facilitates the migration of ions along the polymeric chains.[23]

Scanning electron microscope (SEM) images clearly show the smooth and flat surface of SC-PAM (Fig. 2e and S3), along with

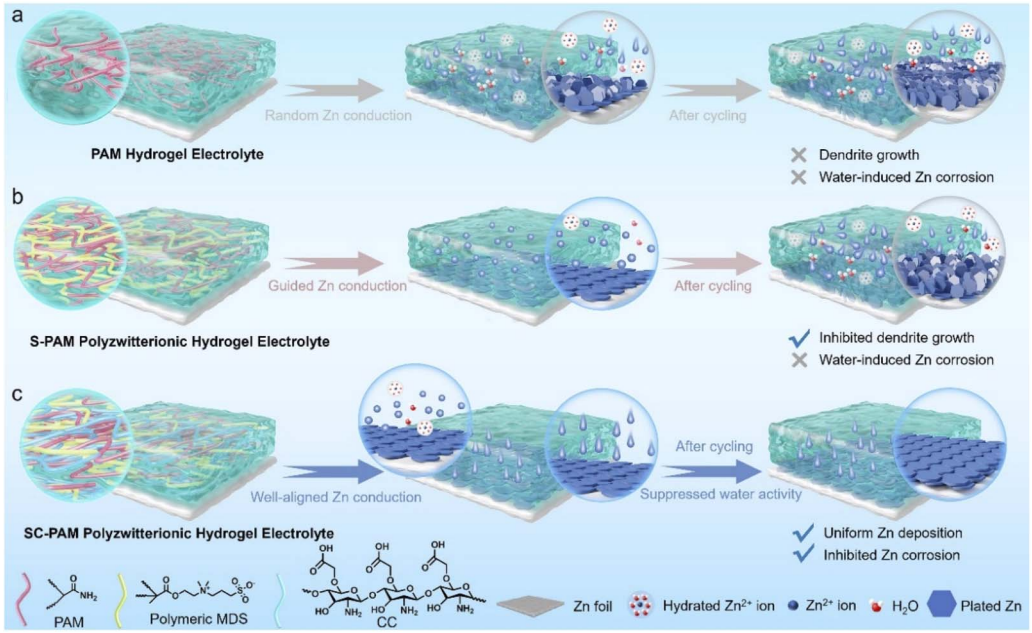

Fig. 1 Schematic illustration of the effects of (a) conventional PAM, (b) S-PAM and (c) SC-PAM hydrogel electrolytes on inhibiting Zn corrosion and dendrite formation.

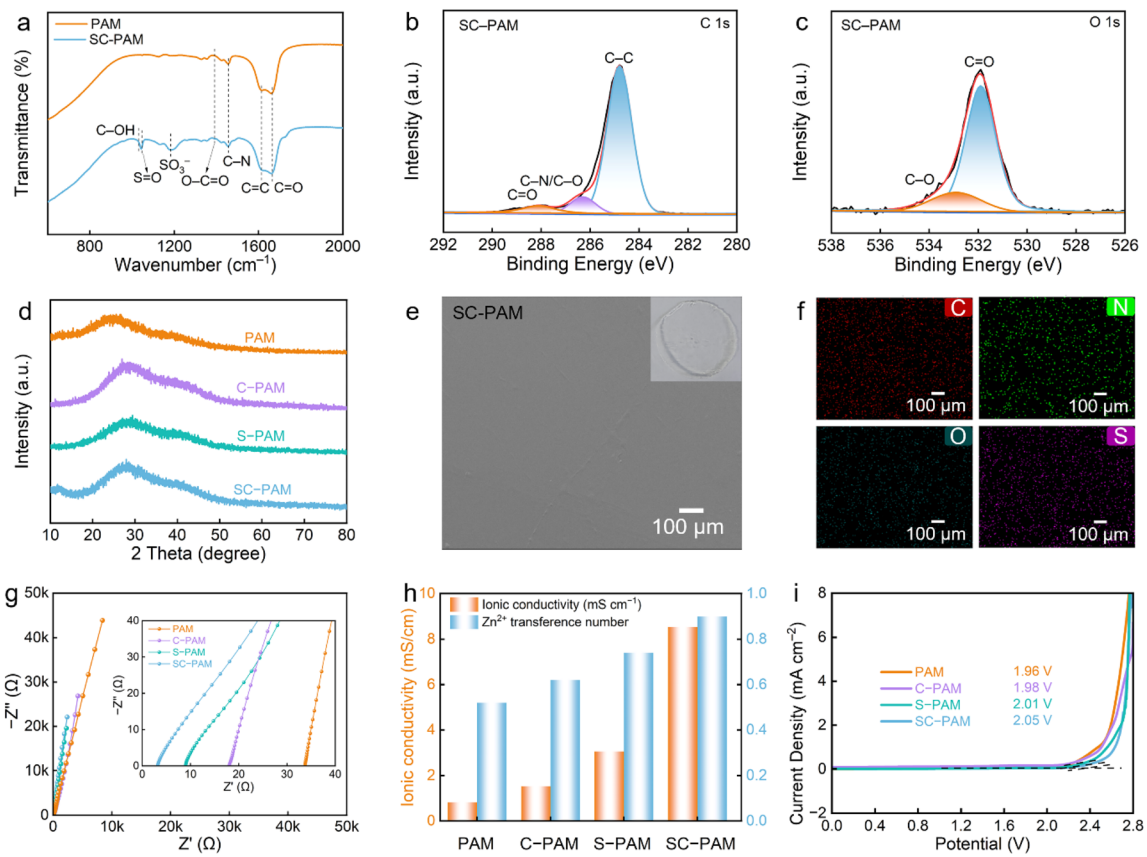

Fig. 2 Structural characterization of S-PAM, C-PAM, S-PAM and SC-PAM hydrogel electrolytes. (a) FT-IR spectra. (b and c) XPS spectra of SC-PAM. (d) XRD patterns. (e) SEM image and (f) EDS images of SC-PAM (inset shows an optical photo of SC-PAM). (g) EIS spectra. (h) The bar chart of ionic conductivity and Zn^{2+} transference number. (i) Linear sweep voltammetry.

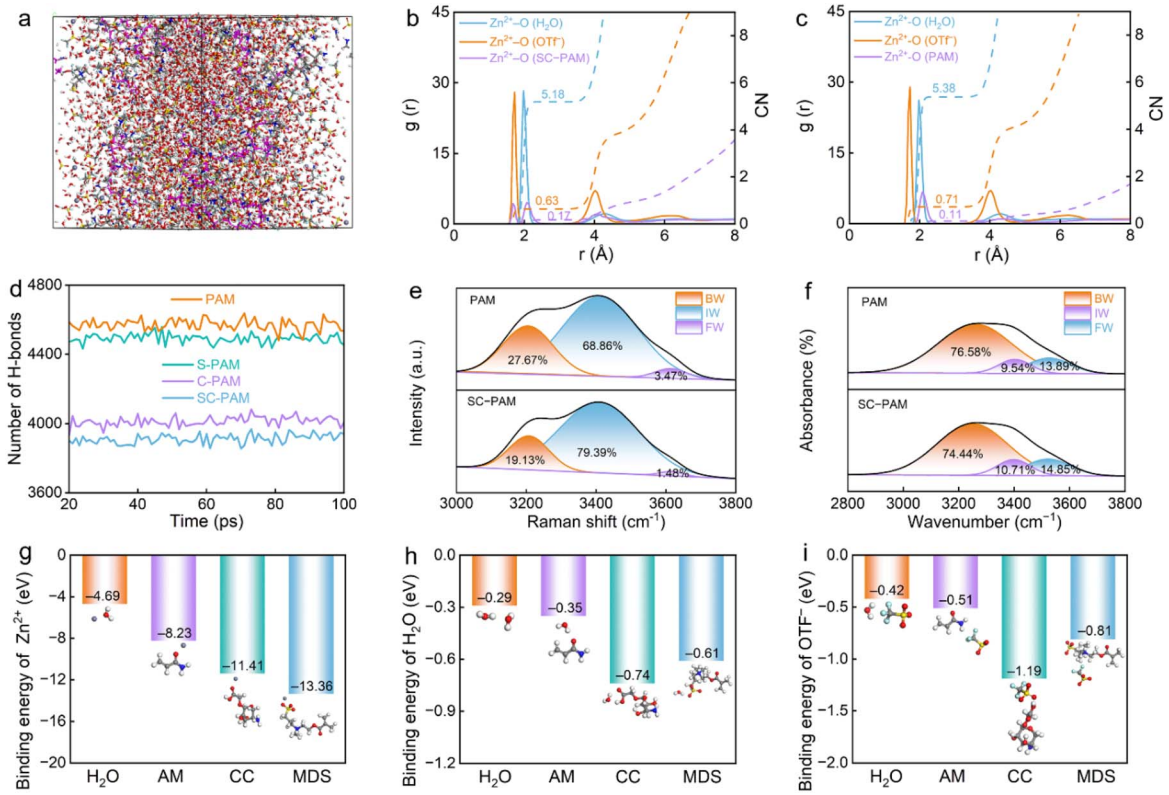

Fig. 3 (a) MD simulation snapshots of SC-PAM and (b and c) RDFs for SC-PAM and PAM. (d) H-bond number of water molecules in PAM and SC-PAM. (e and f) Raman spectra and FT-IR spectra corresponding to Gaussian–Lorentzian fitting. (g–i) Calculated binding energies between Zn^{2+}, H_2O and OTf^- and H_2O, PAM, CC, and MDS.

the homogeneous distribution of C, N, O, and S elements confirmed by energy dispersive spectroscopy (EDS, Fig. 2f). The freeze-dried SC-PAM hydrogel electrolyte shows a porous three-dimensional network structure (Fig. S4a) with the homogeneous distribution of C, N, O, and S elements (Fig. S4b), which can serve as efficient ion-transport channels to facilitate fast Zn^{2+} migration. According to the electrochemical impedance spectra (Fig. 2g), the calculated ionic conductivity of SC-PAM is 8.54 mS cm^{-1} at room temperature, which is much higher than those of S-PAM, C-PAM and S-PAM (0.815–3.05 mS cm^{-1}). The ion migration channels formed by zwitterionic groups in SC-PAM facilitate ion transport, and the polar carboxyl groups with strong electronegativity further enhance the conduction of Zn^{2+} ions (Fig. 2h). Moreover, the Zn^{2+} transference number was measured by using the chronoamperometry (CA) test. Compared with S-PAM, C-PAM and S-PAM (0.52–0.74), the Zn^{2+} transference number (t^{2+}) of SC-PAM is as high as 0.9, reflecting its superior Zn^{2+} migration capability (Fig. 2h, S5 and S6). The increase in the Zn^{2+} transference number can be attributed to the polar carboxyl and sulfonic acid groups in SC-PAM interacting with cations, thereby optimizing the transport behavior of Zn^{2+}.[26,29] The electrochemical stability of SC-PAM as the electrolyte in a Zn‖stainless steel cell was studied *via* linear sweep voltammetry measurement. As expected, SC-PAM possesses a broad electrochemical stable window of ~2.05 V, surpassing those of PAM (1.96 V), C-PAM (1.98 V), and S-PAM (2.01 V) due to suppressed water activity (Fig. 2i).[33]

To investigate the influence of CC and MDS on the solvation structure of SC-PAM, molecular dynamics (MD) simulations were conducted. Radial distribution functions (RDFs) and coordination numbers (CNs) are utilized to illustrate the specific solvation structure of Zn^{2+} ions. The RDFs reveal that Zn^{2+}-O in H_2O possesses a first solvation shell radius of ~1.975 Å, while the solvation shell radius of Zn^{2+}-O in OTf^- is ~1.725 Å. The CN decreases from 5.61 to 5.19 (Fig. 3a–c and S7–S9). Meanwhile, the number of H-bonds between water molecules was quantified in S-PAM, C-PAM, S-PAM and SC-PAM. The H-bond number in SC-PAM is significantly lower than that in the other hydrogel electrolytes (Fig. 3d), indicating that more water molecules are confined in SC-PAM.

The interaction between SC-PAM and water molecules was investigated by deconvoluting the broadband O–H stretching vibration bands in Raman spectra and FT-IR spectra using Gaussian functions, to reveal three distinct states of water molecules (Fig. 3e and f): (I) bound water (BW) at 3253 cm^{-1}, which originates from strongly H-bonding water molecules; (II) intermediate water (IW) at 3451 cm^{-1} associated with disrupted H-bonding and partial hydration networks; and (III) free water (FW) at 3624 cm^{-1} which represents unbound monomers, dimers, or trimers. The proportion of FW in SC-PAM is subsequently reduced, indicating that the incorporation of hydrophilic CC and MDS can effectively promote the conversion of FW to IW and reduce the content of FW, thus inhibiting water activity.[36,37] The contact angles of two hydrogel electrolytes were

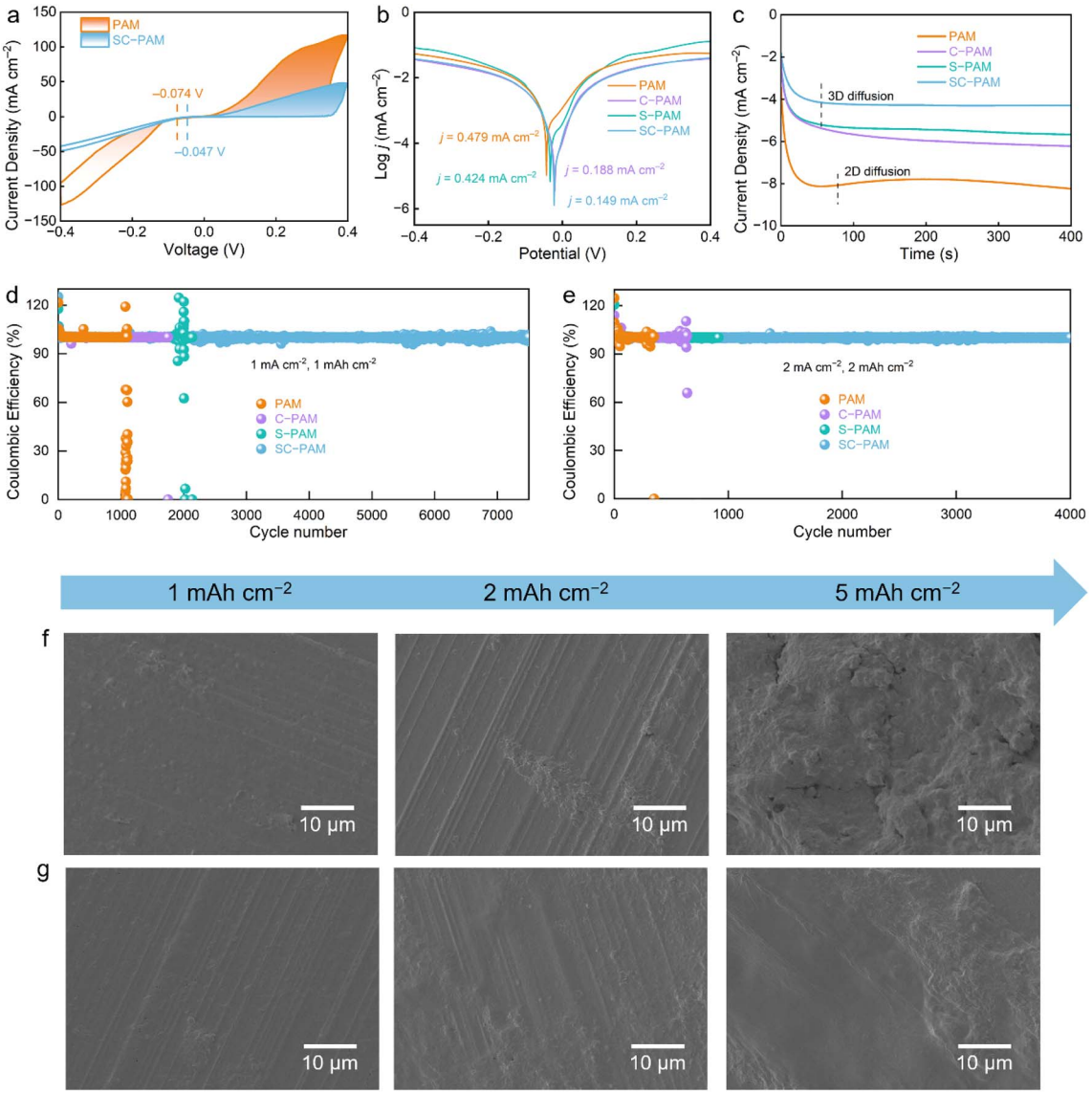

Fig. 4 (a) Cyclic voltammograms of Zn||Cu cells using PAM and SC-PAM hydrogel electrolytes at 1 mV s^{-1}. (b) Tafel plots. (c) CA test of Zn||Zn cells at a constant voltage of −150 mV. (d and e) Long-term performance of Zn||Cu cells. SEM images of plating Zn on a Cu current collector with different areal capacities in (f) PAM and (g) SC-PAM.

measured to reveal their hydrophilicity (Fig. S10), where SC-PAM shows a lower water contact angle of 59° than PAM (84°). This result confirms the efficacy of enhanced hydration in the SC-PAM hydrogel through the incorporation of the strong electronegative carboxyl groups in carboxylated chitosan, which is beneficial for reducing the reaction activity of water to avoid Zn corrosion during the electrochemical process.

Since the major barrier to charge transfer usually arises from the desolvation process of hydrated Zn^{2+} ions, the desolvation behavior of $Zn(OTf)_2/H_2O$, PAM and SC-PAM polyzwitterionic hydrogel electrolytes was further evaluated by calculating the desolvation energy (Fig. S11). The calculation results show that SC-PAM-$[Zn(H_2O)_3OTf]^+$ has a more negative desolvation energy of −18.51 eV than PAM-$[Zn(H_2O)_4OTf]^+$ (−17.06 eV) and $[Zn(H_2O)_6]^{2+}$ (−16.74 eV). Additionally, the thermodynamic stability of the cell is critically influenced by the highest occupied molecular orbital (HOMO) and lowest unoccupied molecular orbital (LUMO) at the electrolyte/Zn anode interface.[38,39] Therefore, the LUMO and HOMO of H_2O, PAM, CC, and MDS were calculated *via* density-functional theory (DFT) calculations. The LUMO energies of MDS (−3.19 eV) and CC (−1.35 eV) in SC-PAM are much lower than that of H_2O molecules (0.019 eV), indicating that the lower LUMO of SC-PAM inhibits the spontaneous reduction of H_2O molecules (Fig. S12).[40]

In SC-PAM, the carboxyl groups of CC and sulfonate groups of MDS exhibit higher theoretical adsorption energies for Zn^{2+} than water (Fig. 3g). An abundance of $-SO_3^-$ and –C═O zincophilic groups in SC-PAM forms an even larger number of lower electronegativity regions, indicating that $-SO_3^-$ and –C═O groups on SC-PAM readily interact with Zn^{2+}. Moreover, calculated binding energies between electrolyte components and

both water molecules/anionic groups show that the formation energies of CC-H_2O and MDS-H_2O are more negative than that of H_2O–H_2O, suggesting that the water molecules tended to interact with the oxygen-containing groups of CC and MDS, thus breaking the inherent H-bonding network between H_2O–H_2O (Fig. 3h and i).[41,42] Moreover, after the introduction of SC-PAM into the solvation structure, the electrostatic potential of the Zn^{2+} solvation structure significantly decreases. As a result, the electrostatic repulsion between Zn cations is reduced, which facilitates the rapid transport of Zn^{2+} ions (Fig. S13).[43,44] In summary, the computational results indicate that both Zn^{2+} and H_2O in SC-PAM prefer to couple with CC and MDS, which breaks the intrinsic H-bonding between free water and regulates the solvated structure of Zn^{2+} ions.[45]

The Zn||Cu cell using SC-PAM polyzwitterionic hydrogel electrolyte exhibits a lower nucleation overpotential (160 mV) than PAM (540 mV), according to the voltage–capacity curves (Fig. S14). This result implies deposition of fine particles of Zn and homogeneous ion transport (Fig. 4a), as also confirmed by cyclic voltammetry (CV). No other peaks in CV profiles can be observed over the voltage window from −0.4 to 0.4 V for Zn plating/stripping, indicating good stability of SC-PAM.[46,47] As evaluated by the Tafel test, the Zn anode in SC-PAM demonstrates the lowest corrosion current of 0.149 mA cm^{-2} (Fig. 4b) in comparison with S-PAM (0.424 mA cm^{-2}), C-PAM (0.188 mA cm^{-2}), and PAM (0.479 mA cm^{-2}). In addition, the Zn^{2+} nucleation and growth behavior on the Zn anode surface in different hydrogel electrolytes were tested using CA curves with a fixed voltage of −150 mV (Fig. 4c). For PAM, the continuous increase

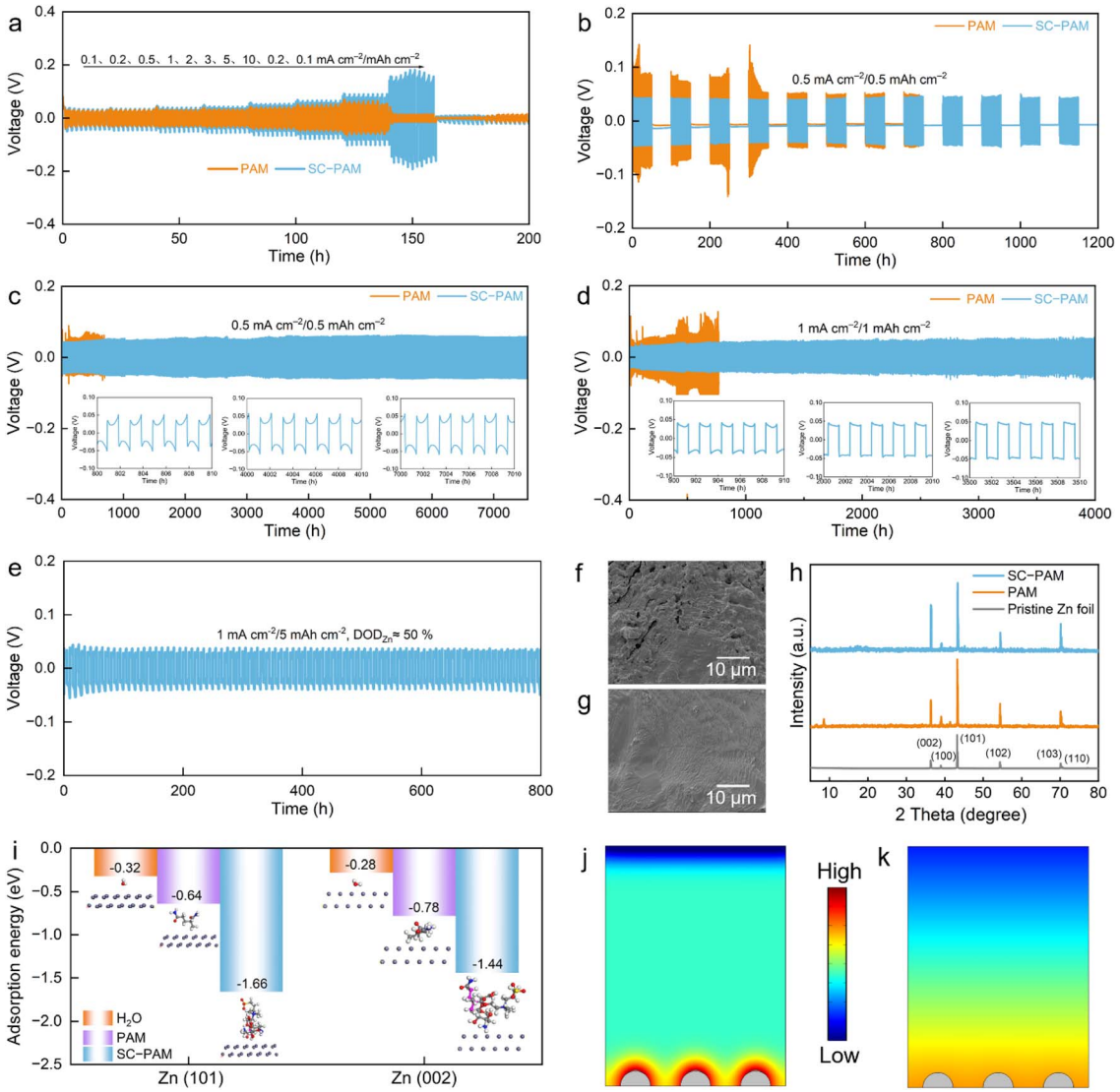

Fig. 5 (a) Voltage profiles of Zn||Zn cells. (b) Cycling performance of Zn||Zn cells during the intermittent galvanostatic charge/discharge test at 0.5 mA cm^{-2}/0.5 mAh cm^{-2}. Voltage profiles of Zn||Zn cells at (c) 0.5 mA cm^{-2}/0.5 mAh cm^{-2}, (d) 1 mA cm^{-2}/1 mAh cm^{-2}, and (e) 1 mA cm^{-2}/5 mAh cm^{-2}. SEM images of the Zn electrodes after 100 cycles at 1 mA cm^{-2} using (f) PAM and (g) SC-PAM. (h) XRD patterns of Zn electrodes after cycling. (i) Adsorption energy of H_2O, PAM and SC-PAM on the (002) and (101) crystal planes of Zn. COMSOL simulations of the Zn^{2+} flux distributions of the Zn electrode with (j) PAM and (k) SC-PAM.

in current density within 300 s indicates that the expansion of effective surface area during nucleation leads to uncontrolled diffusion, which hinders uniform Zn^{2+} nucleation. In contrast, the current density for SC-PAM becomes stable rapidly. This phenomenon is related to the interface protective layer formed on the Zn anode surface, which provides sufficient nucleation sites and induces the unique three-dimensional diffusion of Zn^{2+}, which is beneficial for uniform Zn deposition and can effectively alleviate Zn dendrite formation.[48]

Coulombic efficiency (CE) serves as a key metric for assessing the reversibility of the Zn plating/stripping process. The Zn‖Cu cell using SC-PAM polyzwitterionic hydrogel electrolyte achieves a higher average CE of 99.6% compared to PAM of 86.6%, which is attributed to the effective suppression of parasitic reactions (Fig. S15). Remarkably, the Zn‖SC-PAM‖Cu cell exhibits exceptional long-term stability over 7500 cycles, delivers a high average CE of 99.7% and shows smooth voltage profiles (Fig. 4d). Conversely, the Zn‖Cu cell using PAM hydrogel electrolyte exhibits a significantly shortened cycle life of 1900 cycles, accompanied by a low average CE of 87.9%. This conclusion is further supported by the evolution of Zn deposition morphology, as observed in SEM images (Fig. 4f and g). With the deposition capacity increasing from 1 to 5 mAh cm^{-2}, the Zn anode morphology evolved into vertically oriented flakes (Fig. 4f), the morphology characteristic of a typical two-dimensional diffusion process as inferred from the CA results (Fig. 4c). By contrast, a densely compact and uniformly distributed Zn morphology is achieved in SC-PAM polyzwitterionic hydrogel electrolyte, originating from the parallel stacking and horizontally oriented growth of individual zinc platelets (Fig. 4g). For comparison, we directly coated electronegative chitosan onto the surface of the Zn anode (Fig. S16), showing limited efficacy in inhibiting Zn dendrites and corrosion compared to polyzwitterionic SC-PAM hydrogel electrolyte. These observations demonstrate the effective regulation capability of SC-PAM polyzwitterionic hydrogel electrolyte in Zn nucleation and growth processes.[49,50]

Zn‖SC-PAM‖Zn symmetric cells can withstand large current density fluctuations and exhibit stable and small overpotential with the increased current densities covering a range between 0.1 and 10 mA cm^{-2} (Fig. 5a). Noteworthily, a slight reduction in polarization voltage was observed for the Zn‖SC-PAM‖Zn cell at a reset current density of 0.2 mA cm^{-2} compared to the initial value. After cycling at different current densities, we conducted cycle testing of the battery, which demonstrated excellent cycle stability (Fig. S17). In contrast, the Zn‖PAM‖Zn cell suffers from a short circuit at 10 mA cm^{-2} due to severe dendrites. This further demonstrates the superior rate capability and cycling stability of the Zn‖SC-PAM‖Zn cell. To evaluate the long-term practical potential, the shelf life and recyclability of Zn‖SC-PAM‖Zn batteries were tested by the intermittent galvanostatic (dis)charge test at 0.5 mA cm^{-2}/mAh cm^{-2} (Fig. 5b). The cell maintains an impressive cycling stability over 1200 hours, demonstrating a high stability during (dis)charging.[51,52]

The Zn‖SC-PAM‖Zn cell delivers an overpotential below 100 mV without obvious voltage polarization and continues (dis) charging over 7500 h at 0.5 mA cm^{-2}/mAh cm^{-2}, indicating a stable Zn plating/stripping process, while Zn‖PAM‖Zn cells only maintain 550 h at 0.5 mA cm^{-2}, accompanied by fast short circuits (Fig. 5c and d). Compared with PAM, polyzwitterionic SC-PAM hydrogel electrolyte affords better electrochemical stability for Zn‖Zn cells due to its highly zincophilic-hydrophobic properties. The zincophilic $-SO_3^-$ motifs of sulfobetaine in SC-PAM afford highly Zn^{2+}-selective migration channels to homogenize Zn^{2+} flux. Meanwhile, strong electronegative C=O groups in chitosan strongly anchor H_2O molecules *via* rich H-bonds to form hydrophobic interfacial layers, which shield direct contact between H_2O solvent and the Zn anode to avoid Zn corrosion. The formation of Zn dendrites and passivation between the PAM hydrogel electrolyte and Zn anode are the primary factors leading to cell failure. Moreover, the Zn‖SC-PAM‖Zn cell exhibits a low overpotential of 450 mV and cycling stability at 1 mA cm^{-2}/mAh cm^{-2}. Besides, to evaluate the application potential of SC-PAM in high energy devices with high depth of discharge (DOD), the Zn‖SC-PAM‖Zn cell was evaluated with different levels of (dis)charging measurements employing 10 μm-thick Zn foil. The polarization voltage of the Zn‖SC-PAM‖Zn cell exhibits high stability with a DOD of 30% and 50% (Fig. 5e and S18).

The influence of SC-PAM on the Zn deposition morphology was further investigated by SEM image observation. The Zn electrode surface in the Zn‖PAM‖Zn cell is uneven and consists of flaky agglomerates after 100 cycles (Fig. 5f). In contrast, the deposition morphology of the Zn electrode in the Zn‖SC-PAM‖Zn cell is flat and smooth without obvious protrusions (Fig. 5g). This result proves that SC-PAM effectively induces homogeneous Zn deposition based on electrostatic adsorption, thus effectively suppressing the formation of dendritic protrusions and Zn corrosion and prolonging the electrochemical stability of the Zn anode.[53]

To further investigate the effect of SC-PAM on ion regulation, XRD patterns of the Zn anode in Zn‖Zn cells after cycling were analyzed. The intensity ratio of the diffraction peaks between Zn (002) and (101) indicates that Zn^{2+} ions tend to deposit on the (002) plane of the Zn anode in the Zn‖SC-PAM‖Zn cell, which usually results in a flat Zn anode surface (Fig. 5h).[54] In addition, the Zn anode in the Zn‖SC-PAM‖Zn cell shows diffraction peaks similar to those of pure Zn foil, whereas the Zn anode of PAM-based cells shows diffraction peaks related to by-products. By-products typically result in the creation of cavities and passivation on the Zn anode surface.[55] Furthermore, we tested XRD patterns on the Zn anode surface of the Zn‖SC-PAM‖Zn cell after 500, 1000, 1500, and 2000 h of cycling. The relative peak intensity ratio of the (002) plane to the (101) plane gradually increases with the increase in the cycling time (Fig. S19). It can be seen that the (002) plane becomes the main deposition crystal plane after 500 h of cycling, which indicates the preferential orientation of the Zn deposition plane.[56,57]

To elaborate the mechanism of SC-PAM polyzwitterionic hydrogel electrolyte on Zn deposition behavior, the adsorption energies of H_2O, PAM and SC-PAM on different Zn crystal planes were computed *via* DFT calculations. The results reveal that SC-PAM exhibits significantly stronger adsorption on both (002) and (101) Zn planes (with energies of −1.44 eV eV and

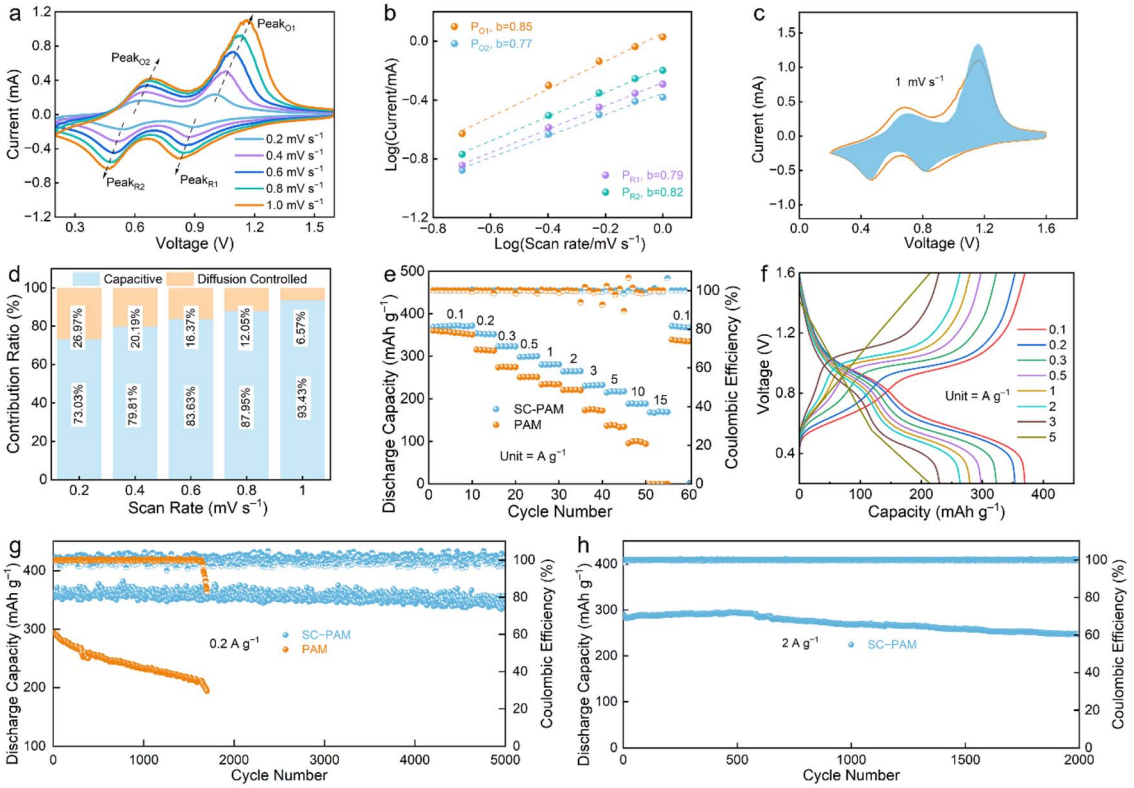

Fig. 6 Charge storage kinetics of the Zn||SC-PAM||V_2O_5 cell. (a) CV curves. (b) Calculated b values. (c) Capacitive contribution at 1 mV s^{-1}. (d) Ratios of capacitive and diffusion-controlled contribution at various scan rates. (e) Rate performance. (f) GCD curves. Long-term cycling performance at (g) 0.2 A g^{-1} and (h) 2 A g^{-1}.

−1.68 eV, respectively) compared to H_2O (−0.32 eV and −0.28 eV) (Fig. 5i). Thus, the preferential adsorption of SC-PAM on the Zn surface regulates the electric double layer and forms a hydrophobic environment, thereby achieving effective anti-corrosion.[58] The slowest Zn^{2+} deposition rate occurs along the (101) Zn planes due to electrostatic repulsion. This is driven by the preferential adsorption of SC-PAM on the (101) plane (−1.68 eV), which exhibits a stronger interaction than the (002) plane (−1.44 eV). Such a feature promotes the exposure of the (002) plane and the formation of preferred (002) deposition textures. This hydrophobic layer can modulate the interfacial ion distribution, eliminate tip effects, and form a water-blocking barrier to mitigate Zn corrosion.[59]

Besides, COMSOL simulations of the Zn^{2+} flux distributions of the Zn electrode confirm the positive effect of SC-PAM on improving zinc deposition behavior. PAM hydrogel electrolyte exhibits an uneven electric field distribution during the initial nucleation stage to trigger the "tip effect", which results in excessive Zn deposition at protrusions and the formation of sharp dendrites (Fig. 5j), while SC-PAM polyzwitterionic hydrogel electrolyte regulates Zn^{2+} ion flux and homogenizes the interfacial electric field distribution (Fig. 5k), enabling the uniform distribution of initial zinc nuclei on the electrode surface thus ensuring subsequent stable zinc deposition.[60,61]

To evaluate the application prospects of SC-PAM polyzwitterionic hydrogel electrolyte, modified V_2O_5 materials (mass loading: ~1.2 mg cm^{-2}) were employed as the cathode to couple with the Zn foil anode to construct the Zn||SC-PAM||V_2O_5 cell. CV curves of the battery show two pairs of peaks at 0.1–1.0 mV s^{-1} covering a range from 0.2 to 1.6 V (Fig. 6a). The dominant role of surface capacitive behavior in the charge storage mechanism is evidenced by the high *b*-values,[62] which corresponds to rapid ion diffusion (Fig. 6b). This result suggests that the redox process involves both diffusion- and capacitive-controlled steps.[63] The rapid capacitive contribution of the V_2O_5 cathode at a scan rate of 1 mV s^{-1} was quantitatively evaluated, demonstrating a high proportion of 93.43% (Fig. 6c). As the scan rate increases, the capacitive contribution from fast surface-redox reactions dominates that of the diffusion-controlled process, rising from 73.03% to 93.43% (Fig. 6d). These results confirm the superior energy storage kinetics of the V_2O_5 cathode. The self-discharge behavior of polyzwitterionic SC-PAM hydrogel electrolyte was investigated at the fully charged state of 1.6 V at 0.2 A g^{-1} (Fig. S20). After standing for 24 hours, the coulombic efficiency of SC-PAM hydrogel electrolyte is as high as 95% compared to PAM (85%). This result indicates the desirable structural stability and practical applicability of SC-PAM hydrogel electrolyte in the Zn||SC-PAM||V_2O_5 battery.

Zn||SC-PAM||V_2O_5 shows a specific discharge capacity of 372 mAh g^{-1} at 0.1 A g^{-1}. The specific capacities of Zn||SC-PAM||V_2O_5 are 372, 352, 323, 299, 280, 265, 230, 216, 189 and 168 mAh g^{-1} at 0.2, 0.3, 0.5, 1, 2, 3, 5, 10 and 15 A g^{-1} respectively. The excellent rate capability is demonstrated by the highly reversible capacity, where specific capacities recovered to

371 mAh g^{-1} when the current rate was reset to 0.1 A g^{-1}.[64] The constant current charge–discharge (GCD) curves of the Zn||SC-PAM||V_2O_5 cell exhibit high capacities (Fig. 6f), owing to the unique polyzwitterionic structure of SC-PAM. Besides, the battery delivers a superior capacity of 353 mAh g^{-1} after 5000 cycles at 0.2 A g^{-1} (Fig. 6g). The V_2O_5 cathode shows identical XRD patterns before and after long-term cycling (Fig. S21), suggesting its unchanged crystal structure during the continuous electrochemical process. Notably, even at a high current density of 2 A g^{-1}, the Zn||SC-PAM||V_2O_5 cell still maintains 99% CE and 84.9% capacity retention after 2000 cycles (Fig. 6h), indicating its outstanding electrochemical cycling stability.

Conclusion

In conclusion, a highly zincophilic-hydrophobic polyzwitterionic hydrogel electrolyte is designed by the crosslinking of strong electronegative zwitterionic sulfobetaine and carboxyl-rich carboxylated chitosan, to regulate uniform Zn^{2+} conduction and suppress Zn corrosion for stabilized Zn anodes. The zincophilic $-SO_3^-$ units of zwitterionic sulfobetaine in SC-PAM provide highly Zn^{2+}-selective diffusion pathways and homogenize Zn^{2+} deposition with a high transference number of 0.90. Meanwhile, electronegative carboxylated chitosan forms a hydrophobic interface on the Zn anode through H-bonding interactions to shield direct contact between H_2O solvent and the Zn anode, thereby inhibiting water-induced corrosion. As a consequence, SC-PAM hydrogel electrolyte endows the Zn||Cu cell with 7600 cycles and a high average CE of 99.7% and the Zn||Zn cell with 7500 h of duration at 1 mA cm^{-2}. Furthermore, the assembled Zn||SC-PAM||V_2O_5 full cell delivers high capacity, high-rate performance, and long lifespan. These findings extend the design concept of zincophilic-hydrophobic polyzwitterionic hydrogel electrolytes for advanced zinc-ion batteries.

Author contributions

M. X. L. conceived the project. L. H. G. and Z. Y. S. supervised the research. J. Z. and Z. Y. S. prepared materials and characterized and analyzed the data. Q. H. performed computational simulation. Y. K. L. assisted in conducting electrochemical analysis. J. Z. and Z. Y. S. wrote the paper. All authors engaged in discussions related to the manuscript.

Conflicts of interest

The authors declare no conflict of interest.

Data availability

The data that support the findings of this study are available on request from the corresponding author, upon reasonable request.

Supplementary information (SI): details of experimental methods, supplementary characterization and electrochemical testing. See DOI: https://doi.org/10.1039/d5sc08853d.

Acknowledgements

This work was financially supported by the National Natural Science Foundation of China (No. 22272118, 22172111, and 22309134), the Shanghai Rising-Star Program (23YF1449200), the Zhejiang Provincial Science and Technology Project (2022C01182), and the Fundamental Research Funds for the Central Universities.

Notes and references

1 D. Larcher and J. M. Tarascon, *Nat. Chem.*, 2015, **7**, 19.
2 A. Innocenti, D. Bresser, J. Garche and S. Passerini, *Nat. Commun.*, 2024, **15**, 4068.
3 Z. Song, W. Liu, Q. Huang, Y. Lv, L. Gan and M. Liu, *Chem. Sci.*, 2025, **16**, 16542.
4 G. Luderer, S. Madeddu, L. Merfort, F. Ueckerdt, M. Pehl, R. Pietzcker, M. Rottoli, F. Schreyer, N. Bauer, L. Baumstark, C. Bertram, A. Dirnaichner, F. Humpenöder, A. Levesque, A. Popp, R. Rodrigues, J. Strefler and E. Kriegler, *Nat. Energy*, 2022, **7**, 380.
5 M. Munjal, T. Prein, M. M. Ramadan, H. B. Smith, V. Venugopal, J. L. M. Rupp, I. I. Abate, E. A. Olivetti and K. J. Huang, *Joule*, 2025, **9**, 101871.
6 W. Yang, Y. Yang, H. Yang and H. Zhou, *ACS Energy Lett.*, 2022, **7**, 2515.
7 Y. Zhang, Y. Fu, Y. Lv, Z. Song, L. Gan and M. Liu, *Chem. Commun.*, 2025, **61**, 14611.
8 J. Han, A. Mariani, S. Passerini and A. Varzi, *Energ Environ. Sci.*, 2023, **16**, 1480.
9 X. Zhao, X. Liang, Y. Li, Q. Chen and M. Chen, *Energy Storage Mater.*, 2021, **42**, 533.
10 S. Lee, J. Hwang, W. Song and S. Park, *Batteries Supercaps*, 2022, **5**, e202200237.
11 H. Li, J. Hao and S. Qiao, *Adv. Mater.*, 2024, **36**, 2411991.
12 C. Liu, X. Xie, B. Lu, J. Zhou and S. Liang, *ACS Energy Lett.*, 2021, **6**, 1015.
13 O. Borodin, J. Self, K. Persson, C. Wang and K. Xu, *Joule*, 2020, **4**, 69.
14 W. Du, Q. Huang, Y. Lv, Z. Song, L. Gan and M. Liu, *Energ Environ. Sci.*, 2025, DOI: 10.1039/D5EE04802H.
15 K. Wu, J. Huang, J. Yi, X. Liu, Y. Liu, Y. Wang, J. Zhang and Y. Xia, *Adv. Energy Mater.*, 2020, **10**, 1903977.
16 D. Mecerreyes, N. Casado, I. Villaluenga and M. Forsyth, *Macromolecules*, 2024, **57**, 3013.
17 R. Wang, M. Yao, S. Huang, J. Tian and Z. Niu, *Adv. Funct. Mater.*, 2021, **31**, 2009209.
18 Y. Lv, Y. Xiao, L. Ma, C. Zhi and S. Chen, *Adv. Mater.*, 2021, **34**, 2106409.
19 H. Zhang, X. Gan, Y. Gao, H. Wu, Z. Song and J. Zhou, *Adv. Mater.*, 2024, **37**, 2411997.
20 Y.-H. Lee, Y. Jeoun, J. Kim, J. Shim, K.-S. Ahn, S.-H. Yu and Y.-E. Sung, *Adv. Funct. Mater.*, 2023, **34**, 2310884.
21 P. Jaumaux, S. Wang, S. Zhao, B. Sun and G. Wang, *Energy Environ. Mater.*, 2023, **6**, e12578.
22 M. Peng, X. Tang, K. Xiao, T. Hu, K. Yuan and Y. Chen, *Angew. Chem., Int. Ed.*, 2023, **62**, e202302701.

23 Y. Cheng, Y. Jiao and P. Wu, *Energ Environ. Sci.*, 2023, **16**, 4561.
24 Y. Lei, F. Liu, L. Chen, M. Xu, Y. Hu, T. Abdiryim, F. Xu, J. You, Y. Tan, Z. Tan and X. Liu, *Nano Energy*, 2025, **143**, 111284.
25 J. Yang, J. Li, J. Zhao, K. Liu, P. Yang and H. Fan, *Adv. Mater.*, 2022, **34**, 2202382.
26 K. Leng, G. Li, J. Guo, X. Zhang, A. Wang, X. Liu and J. Luo, *Adv. Funct. Mater.*, 2020, **30**, 2001317.
27 Q. Fu, S. Hao, X. Zhang, H. Zhao, F. Xu and J. Yang, *Energ Environ. Sci.*, 2023, **16**, 1291.
28 L. Mi and S. Jiang, *Angew. Chem., Int. Ed.*, 2014, **53**, 1746.
29 R. Chen, Q. Liu, L. Xu, X. Zuo, F. Liu, J. Zhang, X. Zhou and L. Mai, *ACS Energy Lett.*, 2022, **7**, 1719.
30 S. Zhang, H. Ao, J. Dong, D. Wang, C. Wang, X. Xu, Z. Hou and J. Yang, *Angew. Chem., Int. Ed.*, 2024, **64**, e202414702.
31 T. Kang, J. Lee, J. Lee, J. Park, J. Shin, J. Ju, H. Lee, S. Lee and J. Kim, *Adv. Mater.*, 2023, **35**, 2301308.
32 W. Zhang, F. Guo, H. Mi, Z. Wu, C. Ji, C. Yang and J. Qiu, *Adv. Energy Mater.*, 2022, **12**, 2202219.
33 O. Zhanadilov, H. Kim, H. Lai, J. Jiang, A. Konarov, A. Mentbayeva, Z. Bakenov, K. Sohn, P. Kaghazchi and S. Myung, *Small*, 2023, **19**, 2302973.
34 T. Wu, C. Ji, H. Mi, F. Guo, G. Guo, B. Zhang and M. Wu, *J. Mater. Chem. A*, 2022, **10**, 25701.
35 Y. Qin, C. Hu, Q. Huang, Y. Lv, Z. Song, L. Gan and M. Liu, *Nano-Micro Lett.*, 2026, **18**, 38.
36 Z. Shen, Y. Liu, Z. Li, Z. Tang, J. Pu, L. Luo, Y. Ji, J. Xie, Z. Shu, Y. Yao, N. Zhang and G. Hong, *Adv. Funct. Mater.*, 2024, **35**, 2406620.
37 Q. He, Z. Chang, Y. Zhong, S. Chai, C. Fu, S. Liang, G. Fang and A. Pan, *ACS Energy Lett.*, 2023, **8**, 5253.
38 S. Cui, W. Miao, X. Wang, K. Sun, H. Peng and G. Ma, *ACS Nano*, 2024, **18**, 12355.
39 H. Lu, J. Hu, X. Wei, K. Zhang, X. Xiao, J. Zhao, Q. Hu, J. Yu, G. Zhou and B. Xu, *Nat. Commun.*, 2023, **14**, 4435.
40 X. Wang, W. Zhou, L. Wang, Y. Zhang, S. Li, X. Li, Z. Zhao, T. Zhang, H. Jin, X. Song, P. Liang, B. Zhang, D. Zhao and D. Chao, *Adv. Mater.*, 2025, **37**, 2501049.
41 Y. Zhang, X. Zheng, N. Wang, W. Lai, Y. Liu, S. Chou, H. Liu, S. Dou and Y. Wang, *Chem. Sci.*, 2022, **13**, 14246.
42 X. Yang, Z. Zhang, M. Wu, Z. Guo and Z. Zheng, *Adv. Mater.*, 2023, **35**, 2303550.
43 A. Khayum M, M. Ghosh, V. Vijayakumar, A. Halder, M. Nurhuda, S. Kumar, M. Addicoat, S. Kurungot and R. Banerjee, *Chem. Sci.*, 2019, **10**, 8889.
44 J. Ke, Z. Wen, Y. Yang, R. Tang, Y. Tang, M. Ye, X. Liu, Y. Zhang and C. Li, *Adv. Funct. Mater.*, 2023, **33**, 2301129.
45 Y. Wang, Q. Li, H. Hong, S. Yang, R. Zhang, X. Wang, X. Jin, B. Xiong, S. Bai and C. Zhi, *Nat. Commun.*, 2023, **14**, 3890.
46 G. Gao, X. Huo, B. Li, J. Bi, Z. Zhou, Z. Du, W. Ai and W. Huang, *Energ Environ. Sci.*, 2024, **17**, 7850.
47 G. Li, Z. Zhao, S. Zhang, L. Sun, M. Li, J. Yuwono, J. Mao, J. Hao, J. Vongsvivut, L. Xing, C. Zhao and Z. Guo, *Nat. Commun.*, 2023, **14**, 6526.
48 B. Li, S. Liu, Y. Geng, C. Mao, L. Dai, L. Wang, S. Jun, B. Lu, Z. He and J. Zhou, *Adv. Funct. Mater.*, 2023, **34**, 2214033.
49 Z. Song, J. Ding, B. Liu, X. Liu, X. Han, Y. Deng, W. Hu and C. Zhong, *Adv. Mater.*, 2020, **32**, 1908127.
50 X. Hu, H. Dong, N. Gao, T. Wang, H. He, X. Gao, Y. Dai, Y. Liu, D. Brett, I. Parkin and G. He, *Nat. Commun.*, 2025, **16**, 2316.
51 Z. Chen, X. Li, D. Wang, Q. Yang, L. Ma, Z. Huang, G. Liang, A. Chen, Y. Guo, B. Dong, X. Huang, C. Yang and C. Zhi, *Energ Environ. Sci.*, 2021, **14**, 3492.
52 S. Yang, Q. Wu, Y. Li, F. Luo, J. Zhang, K. Chen, Y. You, J. Huang, H. Xie and Y. Chen, *Angew. Chem., Int. Ed.*, 2024, **63**, e202409160.
53 H. Wu, S. Zhang, J. Vongsvivut, M. Jaroniec, J. Hao and S. Qiao, *Joule*, 2025, **9**, 102000.
54 J. Cong, X. Shen, Z. Wen, X. Wang, L. Peng, J. Zeng and J. Zhao, *Energy Storage Mater.*, 2021, **35**, 586.
55 X. Li, J. Chen, T. Wang, B. Wang, Y. Cao, D. Chao and Y. Tang, *Angew. Chem., Int. Ed.*, 2025, **64**, e202505855.
56 D. Zhang, Z. Song, L. Miao, Y. Lv, H. Duan, M. Li, L. Gan and M. Liu, *Angew. Chem., Int. Ed.*, 2025, **64**, e202414116.
57 X. Wang, B. Wang, P. Lei, X. Wang, L. Zhou, J. Zhang, J. Zhang and J. Cheng, *Energ Environ. Sci.*, 2024, **17**, 6640.
58 D. Lin, Y. Lin, R. Pan, J. Li, A. Zhu, T. Zhang, K. Liu, D. Feng, K. Liu, Y. Zhou, C. Yang, G. Hong and W. Zhang, *Nano-Micro Lett.*, 2025, **17**, 193.
59 H. Tian, M. Yao, Y. Guo, Z. Wang, D. Xu, W. Pan and Q. Zhang, *Adv. Energy Mater.*, 2024, **15**, 2403683.
60 C. Tian, H. Wang, L. Xie, Y. Zhong and Y. Hu, *Adv. Energy Mater.*, 2024, **14**, 2400276.
61 Y. Dai, W. Du, H. Dong, X. Gao, C. Su, P. Paul, B. Lukic, C. Zhang, C. Ye, J. Li, W. Zong, J. Li, Y. Liu, A. Rack, L. Mai, P. Shearing and G. He, *Nat. Commun.*, 2025, **16**, 7312.
62 K. Guo, Z. Song, Y. Lv, L. Gan and M. Liu, *Adv. Funct. Mater.*, 2025, **35**, 2506036.
63 M. Wu, C. Shi, J. Yang, Y. Zong, Y. Chen, Z. Ren, Y. Zhao, Z. Li, W. Zhang, L. Wang, X. Huang, W. Wen, X. Li, X. Ning, X. Ren and D. Zhu, *Adv. Mater.*, 2024, **36**, 2310434.
64 D. Xu, Y. Wang, H. Tian, Y. Chen, X. Tian and Q. Zhang, *Adv. Energy Mater.*, 2025, **15**, 2502217.